Turkish Journal of Physics

http://journals.tubitak.gov.tr/physics/

Research Article

Turk J Phys
(2019) 43: 459 – 471
© TÜBİTAK
doi:10.3906/fiz-1903-17

First photometric investigation of some ASAS binary systems

Burak ULAŞ*
İzmir Türk College Planetarium, İzmir, Turkey

Received: 21.03.2019 • **Accepted/Published Online:** 29.07.2019 • **Final Version:** 21.10.2019

Abstract: We present the first light curve solutions of the four binary systems observed and catalogued by the All Sky Automated Survey (ASAS) program. The light curves are analyzed by using PHOEBE software, which is based on the Wilson–Devinney method. The light curve parameters are derived and the estimated physical parameters are calculated from the result of the analyses. We compare our targets to well-known binaries of similar type on the Hertzsprung–Russell diagram and mass-radius plane. The evolutionary states of the components are also discussed.

Key words: Eclipsing binary stars, fundamental parameters of stars, stars: individual (ASAS 070530+1521.0, ASAS 073404-3215.9, ASAS 143405-5814.5, ASAS 163424-4919.5)

1. Introduction

The All Sky Automated Survey (ASAS) [1] was set to monitor all sky for stars brighter than 14^m. The project focuses on the photometric variations of selected targets and aims at the classification of the variable stars. The two active telescopes of the project are located in the Las Campanas Observatory, Chile, and Hawaii, USA. The survey is carried out with fully automated equipment with V and I filters and more than 15 million light curves have been catalogued to date.

Binary stars are important tools to understand the stellar lifecycles in the universe. Since most stars are binary stars, binary star studies also allow us to determine the observed universe in terms of stellar evolution and distribution. Semidetached binary systems, in particular, are important for understanding the observed mass exchanges between the components and their effects on the evolutionary properties of the binary stars. They also allow us to reveal the role of binarity in certain phases of the evolution of the stars. Therefore, studies focusing on the derivation of the absolute physical properties and the evolution of binary systems are crucial to figuring out a remarkable part of the observable properties of stars.

Our study is the first detailed investigation of the four binary systems. The information about our targets in the literature is extremely limited. In [2], ASAS 070530+1521.0 were listed in their red and infrared magnitude tables. The target was also catalogued by [3] based on photographs stored at the Warner and Swasey Observatory. In [4] the radial velocity data of ASAS 163424-4919.5 were listed in a survey and the B_T, V_T, J, H, and K magnitudes of the system were provided. The positional and photometric properties of the systems are given in Tables 1 and 2. The effect of the interstellar medium on the light of the systems was derived by using interstellar reddening distribution study in [5]. Considering the calibration of the diagrams and maps in the paper, the galactic coordinates, and distances of our targets, the mean weighted color excess E_y was estimated as $0^m.04$ for A070, $0^m.17$ for A073, between $0^m.1$ and $0^m.2$ for A143, and $0^m.19$ for A163.

*Correspondence: burak.ulas@itk.k12.tr

In the next section, the properties of the light curve data, effective temperature determination, and analyses of the light curves of four binary stars are presented in detail. The third section deals with the results and the location of the components in the HR diagram and mass-radius plane. A brief discussion on the evolutionary status of the systems is made in the last section.

2. Materials and methods

2.1. Properties of the data

The light curves of the targets were obtained in the V passband provided in the ASAS database[1] (Figure 1). They consist of 352, 668, 632, and 567 data points for A070, A073, A143, and A163, respectively. The datasets cover 2544 days for A070, 3298 days for A073, 3189 days for A143, and 3180 days for A163.

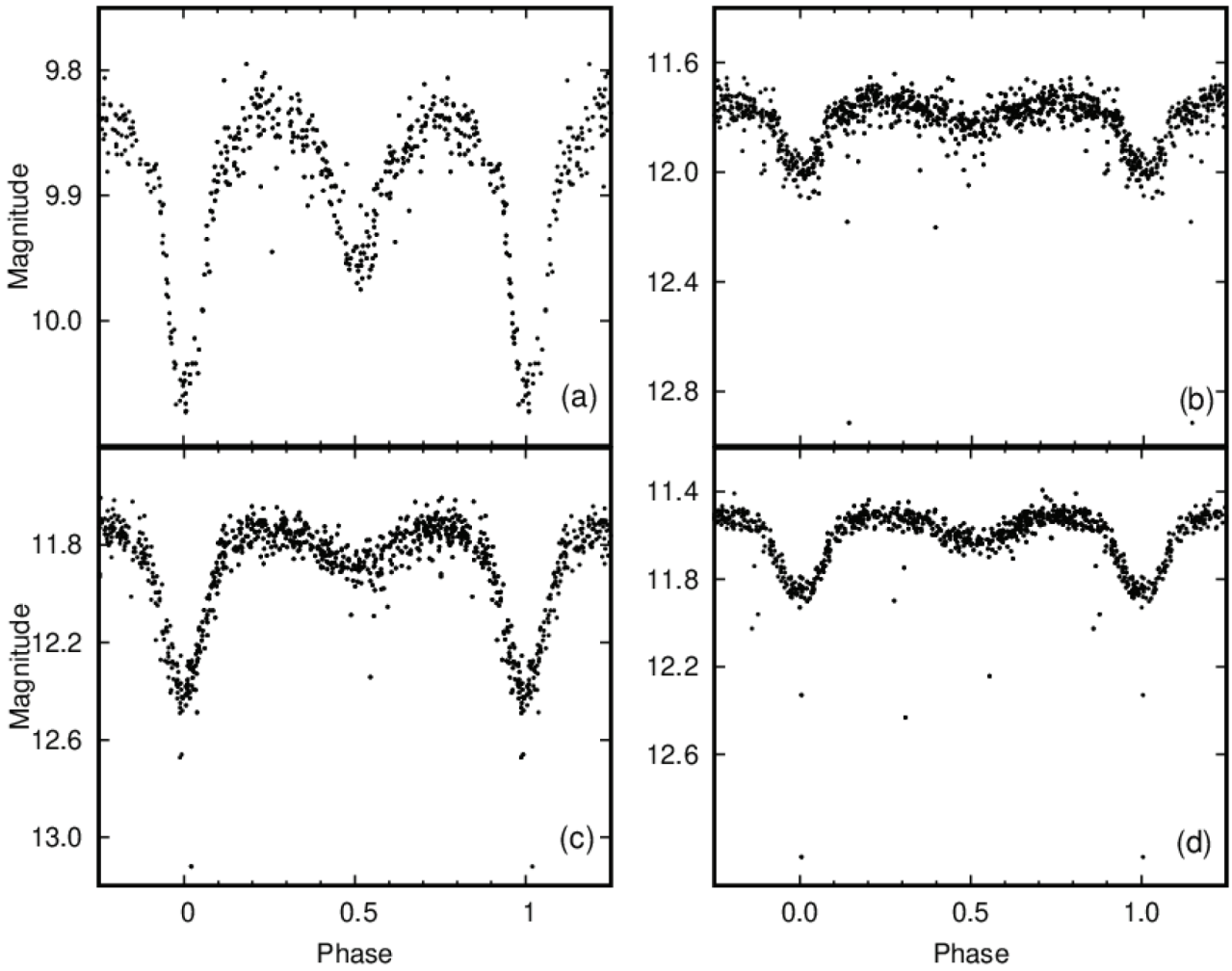

Figure 1. The light curve of system (a) A070, (b) A073, (c) A143, and (d) A163 provided by the ASAS webpage.

[1] www.astrouw.edu.pl/asas.

2.2. Estimation of the effective temperatures

During the light curve analyses of binary stars, the accurate assumption of effective temperatures is critical in order to reveal more realistic results. Therefore, since our targets are not well-studied sources, we made different efforts to achieve the proper assumptions for the effective temperatures of primary components. The spectral type of the system A070, F8V, was given in [3]; therefore, the temperature value to be used in the analysis was estimated from the calibrations given in [6]. The lack of magnitudes obtained during the maximum phases of the light curves of A073 and A143 in the literature directed us to use the effective temperature value given by Gaia DR2 [7,8]. The values are 6368 K and 5861 K for A073 and A143, respectively.

We used $(V-K)_0$ intrinsic color to estimate the temperature value for the target A163. The process was done in five steps: (i) The V magnitude at maximum brightness was taken from the ASAS database. (ii) The K magnitude value was adopted from the 2MASS All-Sky Catalogue of Point Sources [9] by checking the phase of the binary system at the observation time given in the catalogue. According to the catalogue, the 2MASS observation was made during phase 0.79 for A163. Therefore, we ensured that the K magnitude was obtained at the neighboring phase of the system's maximum light. (iii) To calculate the intrinsic $(V-K)_0$ value we used the extinction ratio, k, given in Table 1 of [10]. The authors proposed an equation for the extinction ratio:

Table 1. Positional properties of the systems. RA and DEC stand for equatorial coordinates while l and b are the galactic coordinates. All coordinates are given in J2000 epoch.* Parallaxes are taken from Gaia DR2 [7,8].

ID	ASAS ID	RA (h:m:s)	DEC (°:′:′′)	l (°)	b (°)	Parallax (mas)
A070	070530+1521.0	07:05:30	+15:20:56	200.702	+9.980	2.4571
A073	073404–3215.9	07:34:04	–32:15:54	246.258	–5.984	1.4397
A143	143405–5814.5	14:34:04	–58:14:32	316.114	+1.978	0.6548
A163	163424–4919.5	16:34:24	–49:19:30	335.533	–1.105	1.5175

*simbad.u-strasbg.fr/simbad/.

$$k = \frac{E(color)}{E(BV)}, \tag{1}$$

where *E(color)* is the extinction in any color. It is obvious that the calculation of $E(V-K)$ needs estimation of the $E(B-V)$ color. Thus, we constructed a spectral energy distribution (SED) for the target from the available photometric data in the VizieR database [11]. The photometric data were fit by using a parameter-grid search in order to obtain the optimized Kurucz atmosphere model [12]. Then the $E(B-V)$ value, 0.147, was calculated for A163 from the difference between the reddened and dereddened models. The fit of distribution with the reddened model is shown in Figure 2. A broader explanation of the method of reddening calculation by fitting the SED can be found in [13]. *(iv)* Eq. (1) takes the following form for the $(V-K)$ color [10]:

$$k = \frac{E(VK)}{E(BV)} = 2.71. \tag{2}$$

Therefore, the color excess $E(V-K)$ was determined and $(V-K)_0$ was easily computed by using the relation $(V-K)_0 = (V-K) - E(V-K)$. (v) Finally, we estimated the temperature from Table 11 of [10] by using the $(V-K)_0$ intrinsic value and by assuming that the star is a main sequence star with solar abundance. The

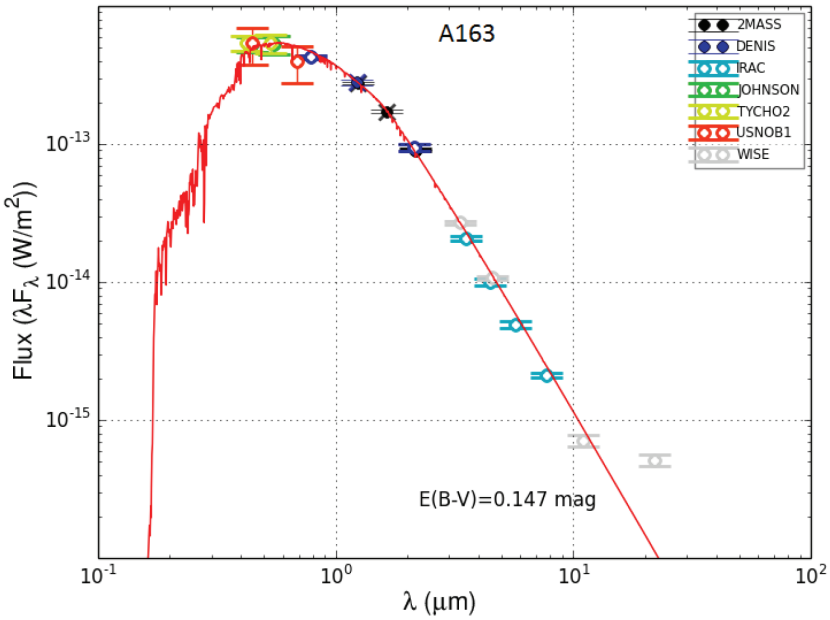

Figure 2. The SED of A163. The legend on the upper right lists the catalogues from which the photometric data were taken. The solid red line indicates the reddened fit using the Kurucz model.

estimated temperature value was used as a fixed parameter during the analysis of the light curve of system A163.

2.3. Analyses of the light curves

The light curves were analyzed separately by using PHOEBE software [14], which uses the Wilson–Devinney method [15]. The program employs the best fit using differential corrections to derive the most appropriate parameters. The systems are classified as semidetached binaries on the ASAS webpage. However, since there is not any other reliable reference on the geometrical configuration of the systems in the literature, we started to analyze the light curves by assuming that the systems are detached binaries. In each step of the analyses, we examined the surface potential values of the components in the case where they exceed the inner or outer critical potential value. Physically meaningful results for systems A070 and A073 were achieved by the assumption of detached configuration, namely Mode 2 of the code. In a certain step of the analysis of A143 in detached binary mode, we encountered a warning message in the output file of the program stating that the secondary component exceeded the critical lobe. Therefore, we reanalyzed the light curve in Mode 5 (semidetached binary, secondary star fills Roche lobe) and obtained physically reasonable results. The most challenging series of analyses were those of A163. We started the analysis in Mode 2, which resulted in the primary component exceeding the outer contact surface and directed us to Mode 4 (semidetached binary, primary star fills Roche lobe). However, a few runs of the program in Mode 4 showed that the secondary component surpassed the critical lobe. Mode 3 (overcontact binary not in thermal contact) of the program was also employed and the code started to give unphysical results for the effective temperature of the secondary component. Finally, physically meaningful results were achieved in Mode 5 (semidetached binary, secondary star fills Roche lobe).

Since there is not any mass ratio (q) value for the systems published in the literature we first applied the q-search technique to the light curves of the systems by using the appropriate modes mentioned in the previous

paragraph in order to derive the appropriate initial mass ratio values. The results of the q-search are shown in Figure 3. We used the q values that corresponded to the minimum χ^2 as the initial mass ratio values for our further analyses.

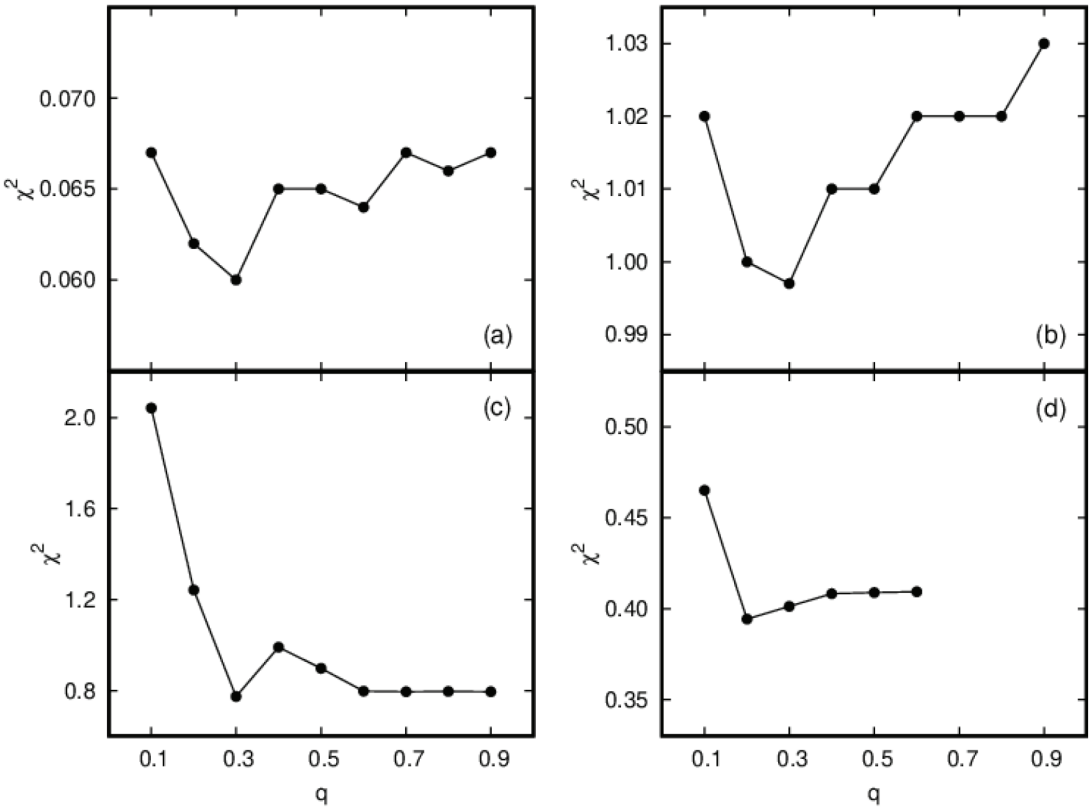

Figure 3. The results of the q-search for (a) A070, (b) A073, (c) A143, and (d) A163. The code gives unphysical results for values higher than 0.6 for A163.

The analyses were applied to the normalized data points. Therefore, before the analyses, the following steps were pursued during the normalization process. We first removed the data points labeled with letters C and D since they are marked as improper or useless in the header of the data files. Then we calculated the phase values for all data by using the ephemerides given on the ASAS webpage. Finally, we generated normalized data points by extracting data points smaller than 1σ and using the average for phase interval $\Delta\varphi = 0.04$. Consequently, we applied the analyses on 25 normalized data points yielded from the data of each target.

The free parameters of the final analyses in Mode 5 were the inclination i, mass ratio q, temperature of secondary component T_2, surface potential of primary component Ω_1, and luminosity of primary component L_1. The surface potential of the secondary component Ω_2 was also set free during the solutions in Mode 2. The $(B-V)$ colors of the binary systems listed in Table 2 indicate that both, or at least one, of their components should have convective envelopes because the granulation boundary for the main sequence stars shows up approximately in spectral type F0 [16], which corresponds to $(B-V)$ =0.3 [6]. Therefore, the gravity darkening coefficients g_1 and g_2 were calculated as in [17] and the albedo values A_1 and A_2 were adopted from [18] by assuming that the components have convective envelopes. The results of the analyses are listed in Table 3. The comparison between the calculated light curves and observations is given in Figure 4.

Table 2. Photometric properties of the systems. T_0 and P are listed by following the values given on the ASAS webpage and they indicate the times of primary minimum and the orbital period, respectively. B_T and V_T magnitudes are taken from the Tycho-2 catalogue [27], while V and K magnitudes are adopted from the ASAS webpage and [28], respectively.

ID	GAIA DR2 ID	TYCHO ID	B_T–V_T (mag)	V–K (mag)	T_0 (days)	P (days)
A070	3359976628178895616	1345-1422-1	0.50	1.22	2452622.1	1.41042
A073	5592279626810866816	7109-2944-1	0.68	1.32	2451930.9	1.554567
A143	5891351393803839360	8691-1308-1	0.31	1.55	2451904.2	1.554567
A163	5940517396305363968	8333-1693-1	0.32	1.47	2451930.9	1.007775

Table 3. The results of the light curve analyses. The standard errors in the last digit are given in parentheses for mass ratio, effective temperature, surface potential, luminosity, and fractional radius. See text for the detailed explanation for the parameters.

Parameter	**A070**	**A073**	**A143**	**A163**
$\mathbf{i(^\circ)}$	74.6(1.9)	77.1(2.3)	82.9(1.8)	87.5(1.8)
$\mathbf{q}$	0.23(3)	0.26(3)	0.33(1)	0.139(7)
$\mathbf{T_1\,(K)}$	6135	6368	5861	6540
$\mathbf{T_2\ (K)}$	5129(138)	4458(212)	3925(130)	4771(139)
$\mathbf{\Omega_1}$	2.5(2)	2.6(1)	2.57(2)	2.21(3)
$\mathbf{\Omega_2\ A_{1,2}\ g_{1,2}}$	2.8(2) 0.5 0.32	2.9(2) 0.5 0.32	$\Omega_{cr}=$ 2.53 0.5 0.32	$\Omega_{cr}=$ 2.08 0.5 0.32
$\frac{\mathbf{L_1}}{\mathbf{L_1+L_2}}$	0.952(3)	0.98(1)	0.98(2)	0.96(1)
$\mathbf{r_1}$	0.441(3)	0.44(3)	0.469(9)	0.51(1)
$\mathbf{r_2}$	0.16(6)	0.16(5)	0.286(4)	0.225(5)

Since the scattering in the light curves may obscure a possible O'Connell effect we investigated the data and examined the trend of out-of-eclipse parts of the curves. The characteristic trace of the effect is that one of the maxima of the light curve is brighter than the other. The factors that cause the O'Connell effect are various: asymmetrically distributed star spots, circumstellar dust and gas, or a hotspot caused by mass transfer [19]. To investigate the effect, we plotted the magnitudes at the maximum phases of the light curves versus cycle numbers (Figure 5). During the process, we limited the range to 0.2–0.3 for the first quadrature and 0.7–0.8 for the second quadrature. We compared the data to the straight lines that intersect the magnitude axes at the maximum value ($9^m.83$ for A070, $11^m.73$ for A073 and A143, $11^m.51$ for A163) that was used for the calculation of the fluxes during light curve analyses. This allowed us to observe the variations in magnitude values from the lines with cycle number. The results indicated that it is not possible to mention notable changes in the lights and the obvious difference between two maxima that can be attributed to the O'Connell effect.

It is also worth pointing out that the fill-out factors, $f = \frac{\Omega_{cr}}{\Omega}\ 1$ [20], for A143 and A163 were found to be –0.01 and –0.05, respectively. These values are very close to those of typical near-contact binary systems [20]. It may be hypothesized that the two systems are near-contact binaries and they can be considered members of the FO Virginis subclass according to the classification of [21] since a remarkable difference between two maxima of the light curves was not detected and the secondary components are at their Roche lobe, i.e. the surface potential values of them are equal to the potential value of the inner contact surface.

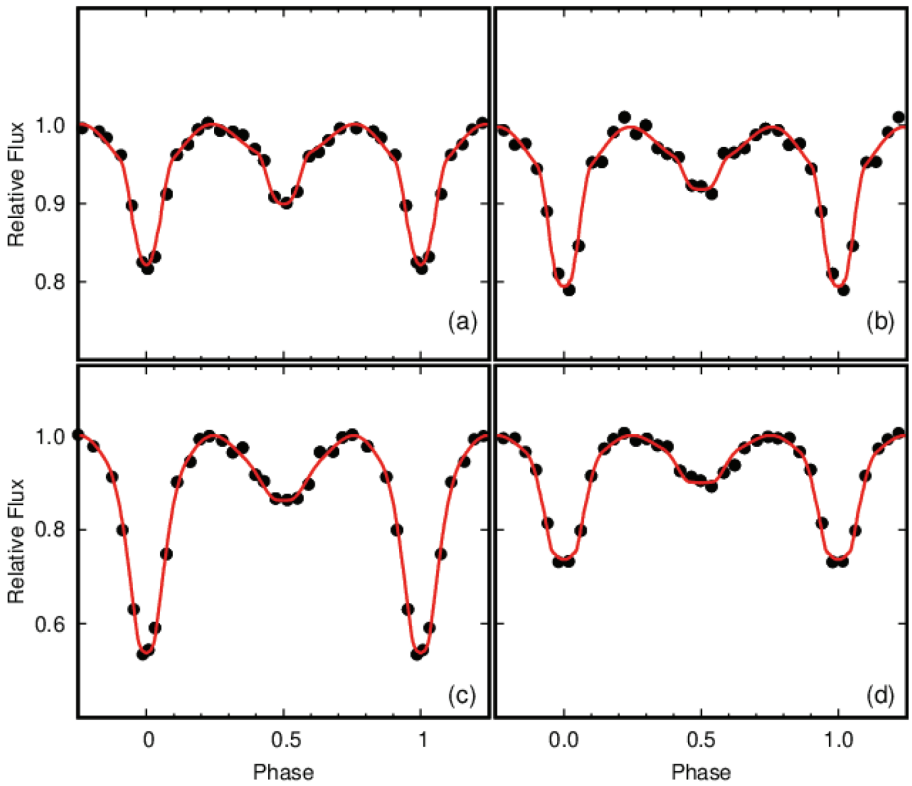

Figure 4. The light curves showing the agreement between observations (dots) and analyses (lines) for (a) A070, (b) A073, (c) A143, and (d) A163.

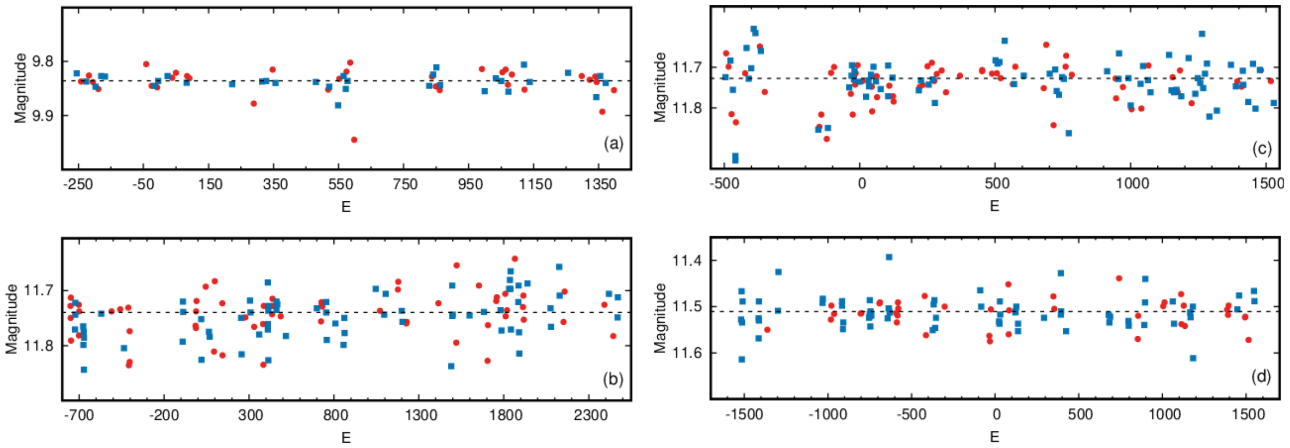

Figure 5. The plots of the fluxes at maximum phases versus cycle numbers (E) for (a) A070, (b) A073, (c) A143, and (d) A163. The red circles and dark blue squares refer to the first and second quadrature data, respectively. The dashed lines intersect the magnitude values at $9^m.83$ for A070, $11^m.73$ for A073 and A143, and $11^m.51$ for A163. Remarkable variations on the data similar to characteristic of O'Connell effect are not observed.

3. Results

The light curve solutions of four binary systems are presented. Our analyses are the first analyses of these systems in the literature. Based on the analyses, we determined the estimated absolute parameters of the systems by using the effective temperature-spectral type-mass calibration of [6] and these are listed in Table 4.

In the determination process we calculated the estimated parameter values by applying interpolation between two neighboring data given by [6]. The geometric models of the components of our targets are also plotted by using the obtained parameters in Table 3 and are shown in Figure 6. These geometric configurations form characteristic detached and semidetached light curves (Figure 4), which show a deep (primary minimum) and a shallow (secondary minimum) minimum. The deeper minimum is observed since the cooler secondary occults the hotter component at about phase 0.0 and hence it causes a decrement in the observed flux value. The shallower minimum, on the other hand, occurs when the cooler component is eclipsed by the hotter one.

Table 4. The estimated absolute parameters of the systems. M, R, T, L, and a correspond to the mass (in solar units), radius (in solar units), effective temperature, luminosity (in solar units), and semimajor axis (in solar radii), respectively. Indices 1 and 2 refer to primary (more massive) and secondary components. The effective temperature of the sun is set to 5777 K [6] during the calculations and the standard errors in the last digit are given in parentheses for mass, radius, effective temperature, semimajor axis, and luminosities of A143 and A163.

Parameter	**A070**	**A073**	**A143**	**A163**
$M_1\,(M_\odot)$	0.9	1.54	1.02	1.3
$M_2\,(M_\odot)$	0.21(3)	0.40(5)	0.34(1)	0.181(9)
$R_1\,(R_\odot)$	2.5(2)	2.4(2)	3.01(6)	2.51(5)
$R_2\,(R_\odot)$	0.9(7)	0.9(5)	1.74(4)	1.05(4)
$T_1\,(K)$	6135	6368	5861	6540
T_2 (K)	5129(138)	4458(212)	3925(130)	4771(139)
$L_1\,(L_\odot)$	8.1(1.2)	8.4(1.2)	9.5(4)	10.2(4)
$L_2\,(L_\odot)$	0.5(7)	0.4(3)	0.64(3)	0.51(4)
a $(R_\odot)$	5.6(1)	5.4(1)	6.40(5)	4.93(3)

Our investigation also covers the comparison of the systems to other systems of similar types. We compare our detached targets, A070 and A073, to 162 detached binaries from [22] and the semidetached systems, A143 and A163, to 61 semidetached Algol-type binaries from [23] on the Hertzsprung–Russell diagram and the mass-radius plane (Figure 7). According to our estimated absolute parameters derived from the analyses and calibrations, it can be mentioned that the secondary components of A070 and A073 show discrepancies from the gathering of the systems of the same type on the mass-radius plane (upper left panel of Figure 7), while they are in good agreement in the Hertzsprung–Russel diagram (upper right panel of Figure 7). The radii of the primary components of the semidetached systems, A143 and A163, seem larger than expected compared to primaries with the same mass (lower left panel of Figure 7) and the secondaries are underluminous compared to the others in the Hertzsprung–Russel diagram (lower right panel of Figure 7).

4. Discussion

Since our systems are found to be detached (A070 and A073) and semidetached (A143 and A163) systems according to our results from the analyses and the calibrations, it is opportune to underline the evolutionary link between these two types of systems: the progenitor of a semidetached binary is a detached system. In a detached system, the more massive component fills its Roche lobe due to its faster evolution. The Roche lobe filling causes the mass transfer to the originally less massive (present primary of semidetached system) component [24]. The mass transfer causes change in the mass ratio and a semidetached system forms when the mass ratio reversal occurs.

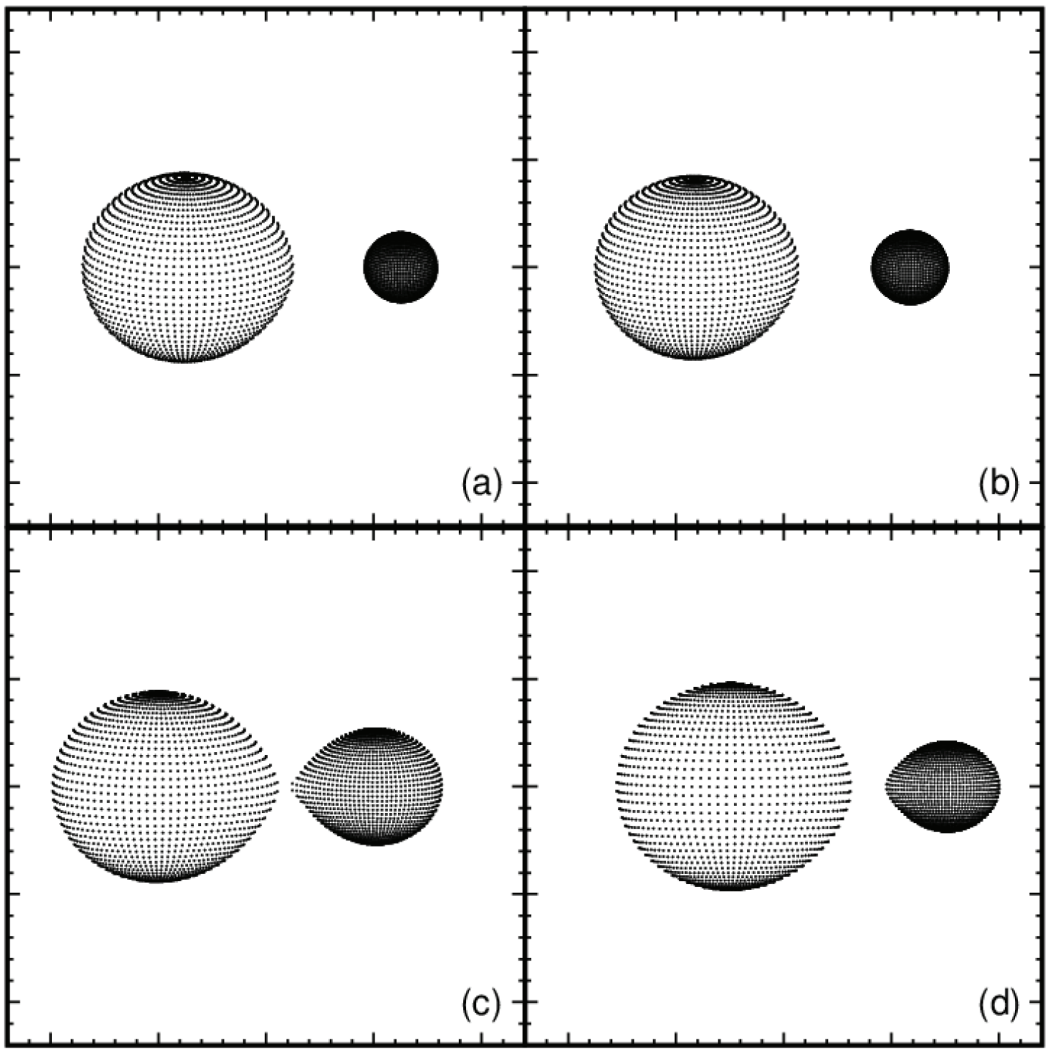

Figure 6. The geometry of the systems for (a) A070, (b) A073, (c) A143, and (d) A163 at phase $\Phi = 0.25$.

We represented the location of our targets with the evolutionary tracks of some binary systems in Figure 8 in order to estimate the evolutionary paths of the systems. These tracks were created by using Binary Star Evolution (BSE) code [25,26]. During the derivation of the evolutionary lines, we set the initial values as follows: eccentricity e_i, between 0 and 1, mass of the primary component M_{1i} between 1.0 $M_\odot$ and 10.0 $M_\odot$, mass of the secondary component M_{2i} between 0.1 $M_\odot$ and M_1, and orbital period of the system P_i between 3 and 7 days. We also limit the maximum evolution time to 15 Gyr. All of the stars in this study were assumed in solar abundances since they are located very near the galactic disk plane as seen from Table 1. In Figure 8, the closest track passing through the location of the components among the thousands of results yielded by running the code was plotted.

Our models for semidetached systems (c and d in Figure 8) show that the evolutionary tracks of the initially less massive components head towards the locations of present more massive components. That is, the current positions of the primaries are on the evolutionary tracks of the initially secondary components. This result also affirms the theory of binary star evolution that we mentioned in the first paragraph of this section.

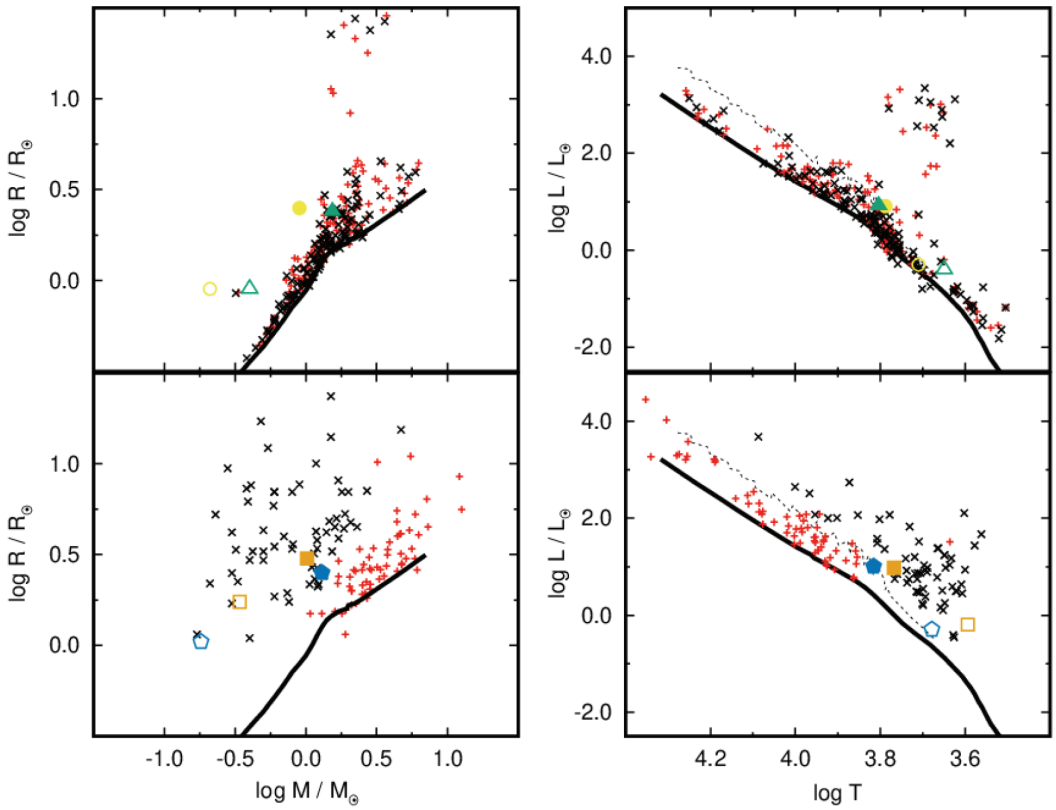

Figure 7. The positions of the components of the systems on the mass-radius plane (left) and the Hertzsprung–Russell diagram (right). The plus and cross symbols refer to the primary and secondary components of detached and Algol-type binaries whose data were taken from [22] and [23]. Circles (yellow), triangles (green), squares (brown), and pentagons (dark blue) indicate the components of A070, A073, A143, and A163, respectively. Filled symbols illustrate the primary components while open ones indicate secondaries. Black solid and dotted lines represent the Zero Age Main Sequence (ZAMS) and Terminal Age Main Sequence (TAMS), whose data are taken from [29].

We conclude that the four targets investigated in this study are detached and semidetached binaries according to our analyses. Spectroscopic observations are crucial for solving the photometric and spectroscopic data simultaneously and deriving more sensitive parameters for the systems in question. More precise values for the parameters will allow us to estimate more accurate scenarios for the evolution of the systems.

Acknowledgments

This research has made use of the SIMBAD database and the VizieR catalogue access tool, operated at CDS, Strasbourg, France. This work has made use of data from the European Space Agency (ESA) mission Gaia (https://www.cosmos.esa.int/gaia), processed by the Gaia Data Processing and Analysis Consortium (DPAC, https://www.cosmos.esa.int/web/gaia/dpac/consortium). Funding for the DPAC has been provided by national institutions, in particular the institutions participating in the Gaia Multilateral Agreement. This publication makes use of data products from the Two Micron All Sky Survey, which is a joint project of the University of Massachusetts and the Infrared Processing and Analysis Center/California Institute of Technology, funded by the National Aeronautics and Space Administration and the National Science Foundation. The author would like to thank the anonymous reviewers for their constructive comments and suggestions.

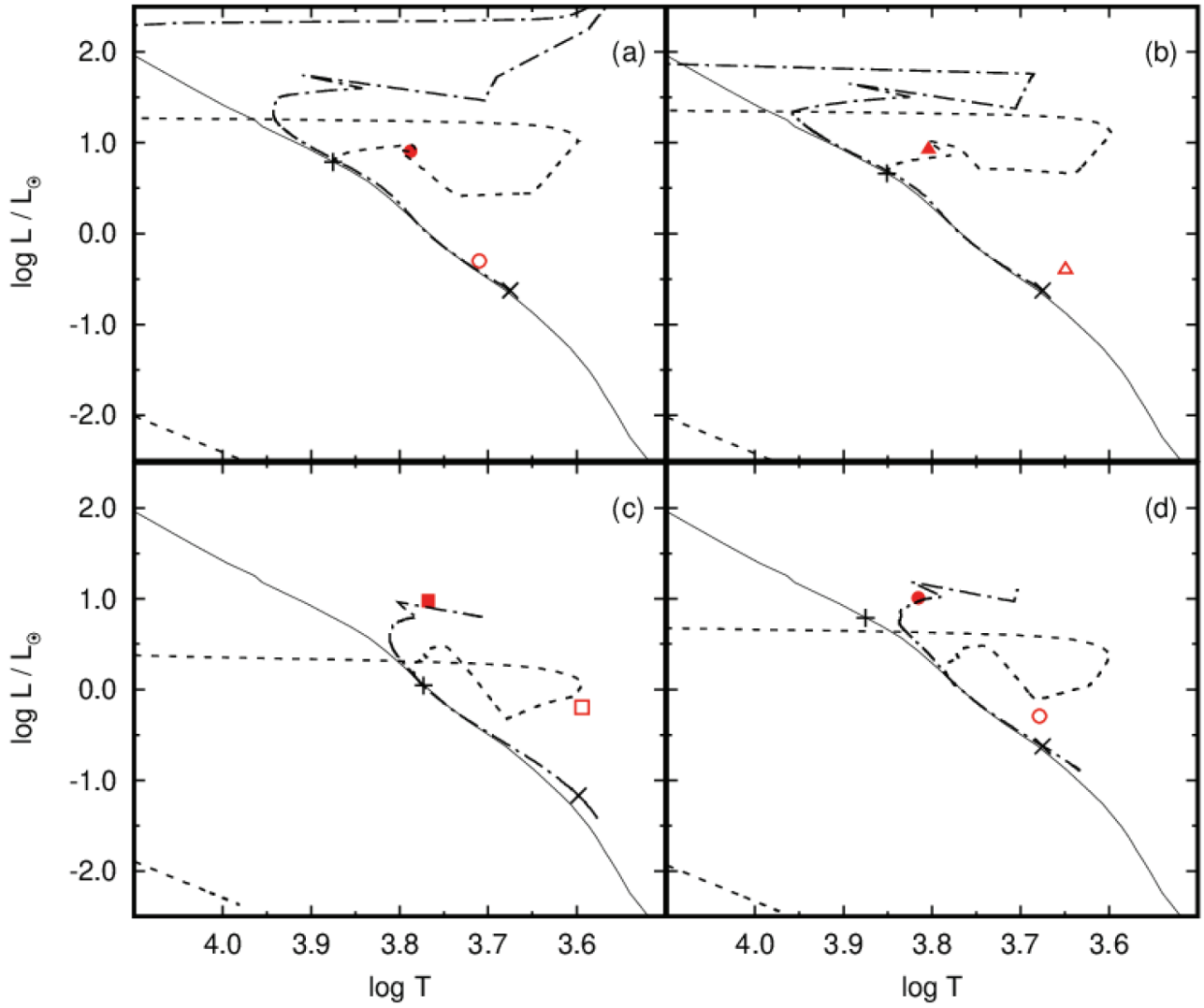

Figure 8. The location of the targets on H–R diagram with the evolutionary tracks of the components of a binary system having initial masses $M_{1i} = 1.6\ M_\odot$, $M_{2i} = 0.8\ M_\odot$, initial period $P_i = 2.4$ days, and initial eccentricity $e_i = 0.6$ for A070 (a); $M_{1i} = 1.5\ M_\odot$, $M_{2i} = 0.8\ M_\odot$, $P_i = 6.0$ days, and $e_i = 0.8$ for A073 (b); $M_{1i} = 1.1\ M_\odot$, $M_{2i} = 0.5\ M_\odot$, $P_i = 6.8$ days, and $e_i = 0.8$ for A143 (c); and $M_{1i} = 1.1\ M_\odot$, $M_{2i} = 0.7\ M_\odot$, $P_i = 2.6$ days, and $e_i = 0.6$ for A163 (d). Filled and open symbols represent the primary and secondary components of the systems, respectively. Plus and cross signs stand for the location of the primary and secondary components of the model in their zero ages. The dashed and dot-dashed lines refer to the evolutionary tracks of primary (more massive) and secondary (less massive) components of the model, respectively. The evolutionary tracks are calculated using BSE code [25,26]. The solid line represents the ZAMS, whose data are taken from [29].

References

[1] Pojmanski G. The All Sky Automated Survey. Catalog of variable stars. I. 0 h - 6 h quarter of the southern hemisphere. Acta Astronomica 2002; 52: 397-427.

[2] Kron GE, Smith JL. Red and infrared magnitudes for 125 stars in ten areas. Astrophysical Journal 1951; 113: 324. doi: 10.1086/145403

[3] Nassau JJ, Macrae DA. Spectral and luminosity classification of the bright sequence stars in the C regions. Astrophysical Journal 1955; 121: 32-37. doi: 10.1086/145960

[4] Frinchaboy PM, Majewski SR. Open clusters as galactic disk tracers. I. Project motivation, cluster membership, and bulk three-dimensional kinematics. Astronomical Journal 2008; 136: 118-145. doi: 10.1088/0004-6256/136/1/118

[5] Fitzgerald MP. The distribution of interstellar reddening material. Astronomical Journal 1968; 73: 983-994. doi: 10.1086/110757

[6] Cox AN. Allen's Astrophysical Quantities. 4th ed. New York, NY, USA: AIP Press, Springer, 2000.

[7] Gaia Collaboration, Prusti T, de Bruijne JHJ, Brown AGA, Vallenari A et al. The Gaia mission. Astronomy and Astrophysics 2016; 595: 1-36. doi: 10.1051/0004-6361/201629272

[8] Gaia Collaboration, Brown AGA, Vallenari A, Prusti T, de Bruijne JHJ et al. Gaia data release 2. Summary of the contents and survey properties. Astronomy and Astrophysics 2018; 616: 1-22. doi: 10.1051/0004-6361/201833051

[9] Cutri RM, Skrutskie MF, van Dyk S, Beichman CA, Carpenter JM et al. VizieR Online Data Catalog: 2MASS All-Sky Catalog of Point Sources. VizieR Online Data Catalog 2003; 2246.

[10] Ramírez I, Meléndez J. The effective temperature scale of FGK stars. II. Teff:Color:[Fe/H] calibrations. Astrophysical Journal 2005; 626: 465-485. doi: 10.1086/430102

[11] Ochsenbein F, Bauer P, Marcout J. The VizieR database of astronomical catalogues. Astronomy and Astrophysics Supplement Series 2000; 143: 23-32. doi: 10.1051/aas:2000169

[12] Kurucz RL. Model atmospheres for G, F, A, B, and O stars. Astrophysical Journal Supplement Series 1979; 40: 1-340. doi: 10.1086/190589

[13] Manick R, Van Winckel H, Kamath D, Hillen M, Escorza A. Establishing binarity amongst Galactic RV Tauri stars with a disc. Astronomy and Astrophysics 2017; 597: 129. doi: 10.1051/0004-6361/201629125

[14] Prša A, Zwitter T. A computational guide to physics of eclipsing binaries. I. Demonstrations and Perspectives. Astrophysical Journal 2005; 628: 426-438. doi: 10.1086/430591

[15] Wilson RE, Devinney EJ. Realization of accurate close-binary light curves: application to MR cygni. Astrophysical Journal 1971; 166: 605-619. doi: 10.1086/150986

[16] Gray DF, Nigel T. The granulation boundary in the H-R diagram. Astrophysical Journal 1989; 341: 421-426. doi: 10.1086/167505

[17] Lucy LB. Gravity-darkening for stars with convective envelopes. Zeitschrift für Astrophysik 1967; 65: 89-92.

[18] Rucinski SM. The proximity effects in close binary systems. II. The bolometric reflection effect for stars with deep convective envelopes. Acta Astronomica 1969; 19: 245-255.

[19] Wilsey NJ, Beaky MM. Revisiting the O'Connell effect in eclipsing binary systems. In: Society for Astronomical Sciences 28th Annual Symposium on Telescope Science; Big Bear Lake, CA, USA; 2009. pp. 107-116.

[20] Bradstreet DH. Fundamentals of solving eclipsing binary light curves using Binary Maker 3. In: Society for Astronomical Sciences 24th Annual Symposium on Telescope Science; Big Bear Lake, CA, USA; 2005. pp. 23-37.

[21] Shaw JS. Near-contact binaries. Memorie della società Astronomia Italiana 1994; 65: 95-103.

[22] Southworth J. DEBCat: A catalog of detached eclipsing binary stars. In: Living Together: Planets, Host Stars and Binaries; Litomyšl, Czech Republic; 2014. pp. 164-165.

[23] İbanoğlu C, Soydugan F, Soydugan E, Dervişoğlu A. Angular momentum evolution of Algol binaries. Monthly Notices of the Royal Astronomical Society 2006; 373: 435-448. doi: 10.1111/j.1365-2966.2006.11052.x

[24] Ritter H. Principles of semi-detached binary evolution. In: Evolutionary Processes in Binary Stars, Proceedings of the NATO Advanced Study Institute; Cambridge, UK; 1996. p. 223.

[25] Hurley JR, Tout CA, Pols OR. BSE: Binary star evolution. Astrophysics Source Code Library 2013; ascl: 1303.014.

[26] Hurley JR, Tout CA, Pols OR. Evolution of binary stars and the effect of tides on binary populations. Monthly Notices of the Royal Astronomical Society 2002; 329: 897-928. doi: 10.1046/j.1365-8711.2002.05038.x

[27] Høg E, Fabricius C, Makarov VV, Urban S, Corbin T et al. The Tycho-2 catalogue of the 2.5 million brightest stars. Astronomy and Astrophysics 2000; 355: 27-30.

[28] Skrutskie MF, Cutri RM, Stiening R, Weinberg MD, Schneider S et al. The two micron all sky survey (2MASS). Astronomical Journal 2006; 131: 1163-1183. doi: 10.1086/498708

[29] Girardi L, Bressan A, Bertelli G, Chiosi C. Evolutionary tracks and isochrones for low- and intermediate-mass stars: from 0.15 to 7 M_{sun}, and from Z=0.0004 to 0.03. Astronomy and Astrophysics Supplement Series 2000; 141: 371-383. doi: 10.1051/aas:2000126